

SUPPORTING INFORMATION

**Accurate Fluorescence Quantum Yield
Determination by Fluorescence Correlation
Spectroscopy**

Daryan Kempe,^{†,¶} Antonie Schöne,[‡] Jörg Fitter,^{*,‡,†} and Matteo Gabba^{*,‡,¶}

*I. Physikalisches Institut (IA), AG Biophysik, RWTH Aachen University, Aachen,
Germany, and Institute of Complex Systems (ICS-5): Molecular Biophysics,
Forschungszentrum Jülich, Jülich, Germany*

E-mail: fitter@physik.rwth-aachen.de; m.gabba@fz-juelich.de

*To whom correspondence should be addressed

[†]RWTH Aachen University

[‡]Forschungszentrum Jülich

[¶]Contributed equally

Contents

1	Theoretical foundations of the MB-method	1
1.1	The MB in the case of pulsed excitation	1
2	Experimental realization of the MB-method	3
2.1	Finding the “low-excitation” intensity regime	3
2.2	Determination of the MB values of fluorescent molecules	4
2.3	Determination of the integrated transmission parameter g	8
3	Theoretical Foundation of the τ-Method	10
4	Experiments and Data analysis	12
4.1	“Low-excitation” intensity regime	12
4.2	Results of the MB-method	12
4.3	Results of the τ -method	13
4.4	Derivation of the quenching constants	14
5	Estimation of the Sample Consumption	15
	Bibliography	18

1 Theoretical foundations of the MB-method

1.1 The MB in the case of pulsed excitation

For a pulsed excitation, the dependency of $k_f(\vec{r})$ on the excitation intensity distribution is given by:¹

$$k_{f,p}(\vec{r}) = \frac{QY \cdot k_{10} \cdot J(\vec{r})}{1 + J(\vec{r}) \cdot \frac{k_{isc}}{k_T}} \quad (\text{S1})$$

with

$$J(\vec{r}) = \frac{k_{ex}}{k_s} \cdot \frac{T_p}{T_r} + \frac{k_{ex}^2}{k_s^2 \cdot T_r \cdot k_{10}} \cdot \frac{[1 - e^{(-k_s \cdot T_p)}] \cdot [1 - e^{(-k_{10} \cdot \Delta T)}]}{[1 - e^{(-k_{10} \cdot T_r - k_{ex} \cdot T_p)}]} \quad (\text{S2})$$

and the short-hand notations $k_{ex}=k_{ex}(\vec{r})=I_{0,p} \cdot EID(\vec{r}) \cdot \sigma$, $k_s=k_s(\vec{r})=k_{ex} + k_{10}$ and $\Delta T=T_p - T_r$. Here, $I_{0,p}$ denotes the applied excitation intensity for a pulsed excitation, and k_{10} denotes the de-populating rate constant from the the first excited state to the ground state. T_p and T_r are the length and the repetition period of the laser pulses, respectively. Here, it should be mentioned that

$$I_0 = I_{0,p} \cdot \frac{T_p}{T_r}, \quad (\text{S3})$$

where I_0 denotes the applied excitation intensity in the case of cw-excitation. In analogy with the case of cw-excitation, by assuming “low-excitation” intensities, Equation S2 can be approximated to get a linear dependency on the excitation intensity again:

$$J(\vec{r}) \approx \sigma \cdot \frac{1}{k_{10}} \cdot \frac{T_p}{T_r} \cdot EID(\vec{r}) \cdot I_{0,p} \quad (\text{S4})$$

For small excitation rates, J is small as well, and Equation S1 can be approximated linearly:

$$k_{f,p}(\vec{r}) \simeq QY \cdot k_{10} \cdot J(\vec{r}) \quad (\text{S5})$$

Inserting eq. S4 into eq. S5 leads to:

$$k_{f,p}(\vec{r}) \simeq QY \cdot k_{10} \cdot \sigma \cdot \frac{1}{k_{10}} \cdot \frac{T_p}{T_r} \cdot I_{0,p} \cdot EID(\vec{r}) \quad (\text{S6})$$

which can be simplified to an expression

$$k_{f,p}(\vec{r}) \simeq QY \cdot \sigma \cdot I_0 \cdot EID(\vec{r}) \quad (\text{S7})$$

coinciding with Equation 4. Therefore, the subsequent steps are identical to the steps reported in the main text for cw excitation leading to Equation 7.

2 Experimental realization of the MB-method

Based on the theoretical framework given in the previous sections, the experimental realization of the MB-method is specified in this section. In other words, the determination of all input parameters entering Equation 7 is described in detail.

2.1 Finding the “low-excitation” intensity regime

As mentioned before, Equation 7 is only applicable when the applied excitation intensity I_0 is sufficiently low to ensure a linear dependency of k_f with respect to I_0 . To assess this “low-excitation” intensity regime, Equations 3, 4 and S1 are calculated as functions of I_0 and plotted together. The intensity range where the three curves coincide represents the “low-excitation” intensity regime. An exemplary result is shown in Figure S1 for the case of Fluorescein in 0.1M NaOH. The parameters σ and τ entering the equations are directly assessable. The absorption cross section σ can be derived from the molar absorption coefficient using the linear relation between the two quantities ($\sigma = 2,303 \cdot \epsilon/N_A$),² and the fluorescence lifetime τ can be determined by the analysis of a fluorescence lifetime decay.³ As opposed to this, the rates k_{isc} and k_T are rather difficult to determine.⁴ Fortunately, only their ratio affects the course of the curve. Here, it was fixed to a rather large value of 10 which is equal to or higher than the values expected for the dyes used in this paper.⁵⁻⁷ As the deviation from a linear response increases when the ratio of k_{isc} to k_T becomes larger, our choice ensures that the “low-excitation” regime is chosen reasonably. Apparent from Figure S1, this regime of I_0 lies between 0 and $2 \frac{kW}{cm^2}$. To identify the laser power range corresponding to the “low-excitation” intensity regime, the following equation was used:

$$P_0 = \pi \cdot \omega_0^2 \cdot I_0 \cdot \frac{1}{2} \tag{S8}$$

Here, P_0 denotes the laser power and ω_0 denotes the waist of the focused laser beam. Under the assumptions that the unfocused beam is Gaussian and under-filling the back-aperture of

the objective, ω_0 can be predicted according to:⁸

$$\omega_0 = \frac{\omega}{\left(1 + \left(\frac{z_0}{f}\right)^2\right)^{0.5}} \quad (\text{S9})$$

with

$$z_0 = \frac{\pi \cdot \omega^2}{\lambda_{ex}} \quad (\text{S10})$$

Here, ω denotes the waist and z_0 the Rayleigh range of the unfocused laser beam entering the back-aperture of the objective. The focal length of the objective is denoted by f . For details on the maximum laser powers used in this work see Section 4.1.

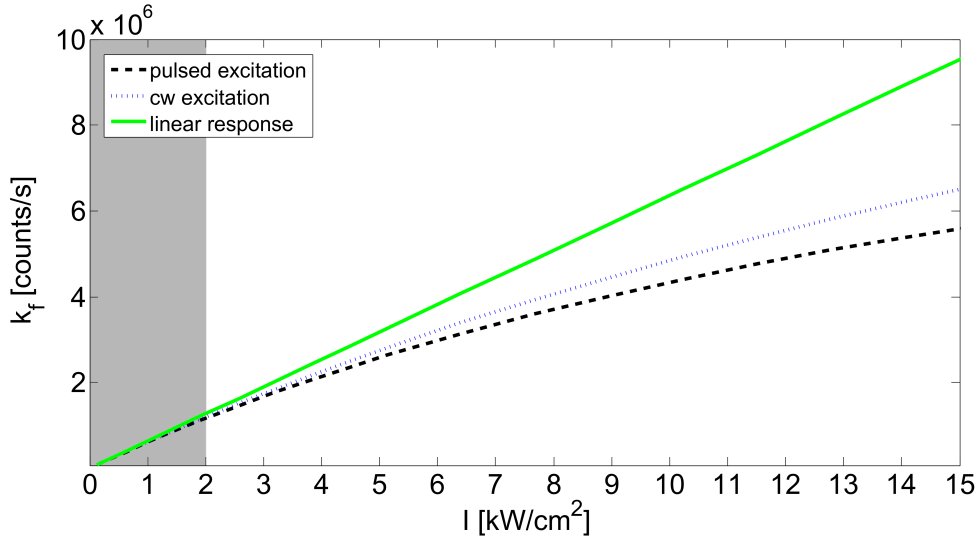


Figure S1: Calculated fluorescence count-rates k_f as a function of the applied excitation intensity I_0 for Fluorescein in 0.1 M NaOH. The green curve corresponds to k_f being linearly dependent on I_0 . The blue curve corresponds to k_f being excited continuously whereas the black curve predicts k_f in the case of pulsed excitation. In grey the “low-excitation” intensity regime is highlighted, being equivalent to the range where the three curves coincide. The input parameters are $\sigma = 2.82 \times 10^{-16} \text{ cm}^2$, $\tau = 4.1 \text{ ns}$, $\frac{k_{isc}}{k_T} = 10$.

2.2 Determination of the MB values of fluorescent molecules

As was mentioned before, the slope m entering Equation 7 is obtained from linear least-squares fitting of the measured MB-values plotted as a function of the applied excitation

intensity. Experimentally, the MB can be determined by taking the ratio of the measured overall fluorescence count-rate of a sample, F , to the average number of fluorescent particles present in the detection volume $\langle N \rangle$. F is obtained by calculating the mean of the binned fluorescence intensity time trace (see Figure S2).

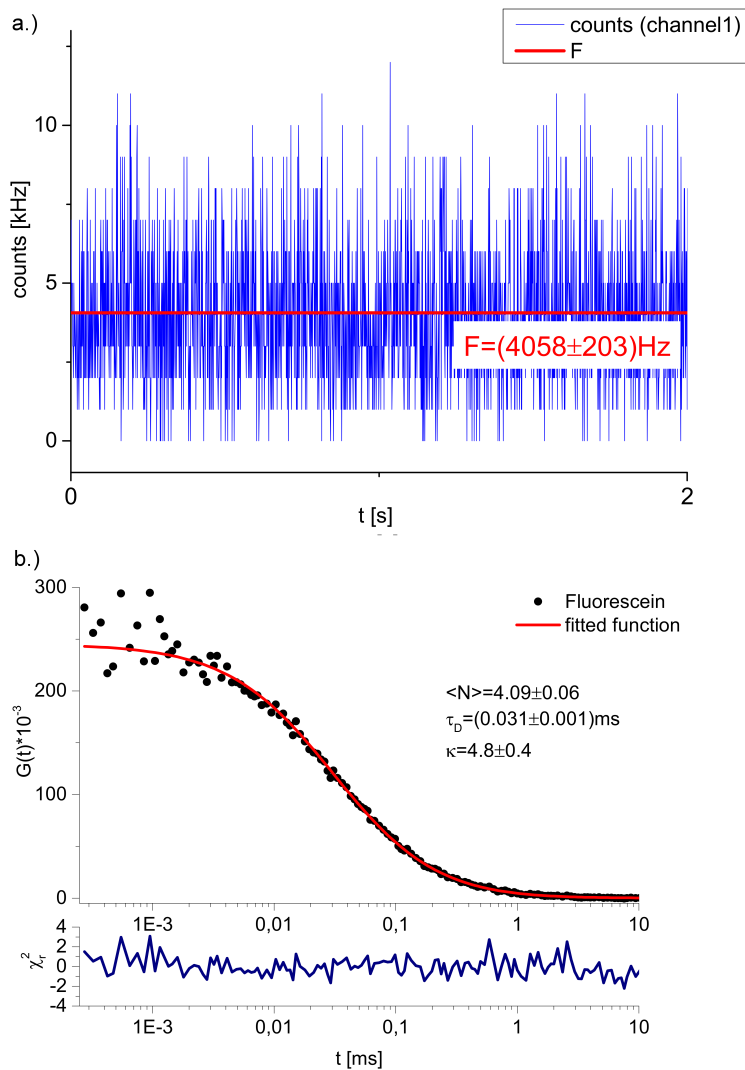


Figure S2: a.) Time trace obtained measuring Fluorescein in 0.1 M NaOH. The mean fluorescence count-rate F is shown in red b.) Auto-correlation-curve of Fluorescein in 0.1 M NaOH analyzed using Equation S16. The resulting fitted model curve is given in red. The weighted reduced residuals are given in dark blue. The applied laser power was $0.71 \mu\text{W}$.

Obviously, F equals the sum of the fluorescence count-rate originating from the fluorescent sample and the signal generated by the solvent, BG. As all measurements here are performed

at low excitation intensities ($< 2 \frac{kW}{cm^2}$), the influence of BG should be taken into account^{9,10}

$$F_c = F - BG. \quad (S11)$$

BG is obtained by simply measuring the count-rate generated by the pure solvent applying the same excitation intensity used to measure the actual sample. The parameter $\langle N \rangle$ is not directly assessable but can be extracted by analyzing the auto-correlation of the measured time trace (FCS-curve). Besides $\langle N \rangle$, the diffusion time of the fluorescent particles, τ_D , the eccentricity of the detection volume, κ , as well as potential photophysical processes determine the course of a FCS curve $G(t)$:¹¹

$$G(t) = \frac{1}{\langle N \rangle} \cdot \frac{1}{(1 - T)} \cdot \frac{1}{(1 + \frac{t}{\tau_D})} \cdot \frac{1}{(1 + \frac{t}{\tau_D \cdot \kappa^2})^{\frac{1}{2}}} \cdot (1 - T + T \cdot e^{-\frac{t}{\tau_T}}) \quad (S12)$$

Here, T denotes the fraction of particles that have entered the triplet state and τ_T denotes the corresponding triplet state relaxation time. By fitting Equation S12 to the experimentally obtained correlation curve, $\langle N \rangle$ can be obtained. Again, the influence of the background count-rate BG has to be taken into account:^{9,10}

$$\langle N \rangle_c = \frac{\langle N \rangle}{(1 + \frac{BG}{F_c})^2} \quad (S13)$$

The MB is then calculated using the following equation:

$$\boxed{MB = \frac{F_c}{\langle N \rangle_c}} \quad (S14)$$

Apparently, the reliability of the determined MB depends on the reliability of the determined F_c and $\langle N \rangle_c$. On the one hand that means that the measured mean fluorescence count-rate should not vary too much during the recording time. On the other hand, the parameter $\langle N \rangle$ should not be biased by the outcome of other fitting parameters entering Equation S12.

More specifically, parameters contributing rather little to the course of the FCS-curve can fluctuate strongly in terms of their attained value, thereby changing the outcome of $\langle N \rangle$. In this regard, attention should be paid to the triplet fraction parameter T . Its dependency on the excitation intensity is given by:²

$$T = \frac{\sigma \cdot I_0 \cdot k_{isc}}{\sigma \cdot I_0 \cdot (k_{isc} + k_T) + k_T \cdot (k_{isc} + k_{10})} \quad (\text{S15})$$

The triplet fraction as a function of the excitation intensity and the ratio k_{isc}/k_T is shown in Figure S3 for Fluorescein in 0.1M NaOH.

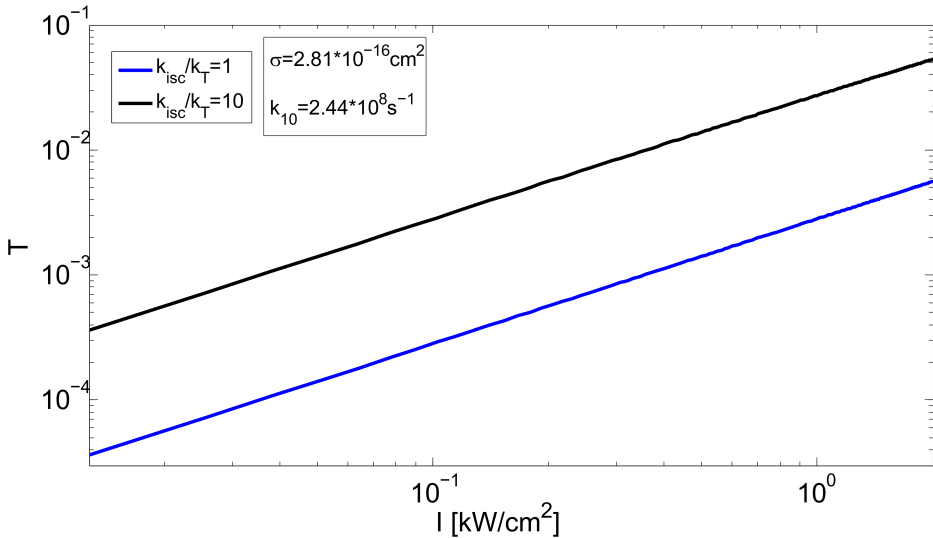


Figure S3: Triplet state fraction T as a function of the excitation intensity I_0 for the case of Fluorescein in 0.1 M NaOH; the ratio of k_{isc} to k_T is varied from 1 to 10 to show its impact on the course of the curve; the other input parameters are $\sigma = 2.82 \times 10^{-16} \text{ cm}^2$ and $\tau = 4.1 \text{ ns}$.

For the calculation, input parameter values taken from the literature were used. Applying excitation intensities below $2 \frac{kW}{cm^2}$, the calculation shows that triplet fractions below 6% are obtained even in the (extreme) case when k_{isc} is ten times larger than k_T . As a consequence, the triplet fraction showing up in the “low-excitation” intensity FCS curves is hardly visible by eye and can, when treated as a free parameter during the fitting procedure, fluctuate strongly in terms of its fitting value. This problem can be circumvented by limiting the

range of values of T or even fixing T to one specific value during the fitting procedure. First, the data sets were fitted using model Equation S12 with T fixed to values around 6%. Second, to test whether the outcome of $\langle N \rangle$ changes when T is not taken into account at all, the same data sets were fitted using a model without any triplet state parameters entering:

$$G(t) = \frac{1}{\langle N \rangle} \cdot \frac{1}{\left(1 + \frac{t}{\tau_D}\right)} \cdot \frac{1}{\left(1 + \frac{t}{\tau_D \cdot R^2}\right)^{\frac{1}{2}}} \quad (\text{S16})$$

Since the difference in the outcome parameter $\langle N \rangle$ lied below 1%, the simpler Equation S16 was used to fit all of the data-sets with the exception of Alexa647-related samples. Alexa647 belongs to the family of carbocyanine dyes¹² for which, at low excitation intensities, the most important photo-physical process affecting the (sub)-microsecond regime is the so-called photo-induced cis/trans-isomerization. For this process, the fraction of molecules in the dark trans-state is not dependent on the applied excitation intensity.¹³ As a matter of fact, even for FCS-curves originating from “low-excitation” intensity measurements, a constant dark-state fraction of around 30% shows up which is clearly visible by eye and well-separated from the diffusion-related part of the curve. Therefore, all FCS-curves of Alexa647 could be fitted without any constraints using Equation S12.

An exemplary result of a “low-excitation” intensity time trace measurement is given in Figure S2 for the case of Fluorescein in 0.1M NaOH.

2.3 Determination of the integrated transmission parameter g

In a confocal microscope setup, the emitted fluorescence light is attenuated by several optical elements in the light path (e.g. objective, dichroic mirror(s), emission filters), as well as by the non-perfect quantum efficiency of the detectors. To which extent light is attenuated by a specific component is quantified by its wavelength dependent transmission/efficiency spectrum having values between 0 and 1. By multiplying the transmission/efficiency spectra of all components with each other, a system specific overall transmission spectrum g_λ can

be calculated.

The fraction of the fluorescence emission of a specific dye that is transmitted/detected is quantified by the transmission parameter g . To determine g , the fluorescence spectrum of the dye has to be measured and normalized to an integrated intensity of one. The normalized spectrum is then multiplied with the transmission spectrum g_λ . Finally, the resulting product is integrated over all wavelengths to calculate the transmission parameter g . This is exemplarily depicted in Figure S4 for Fluorescein in 0.1M NaOH.

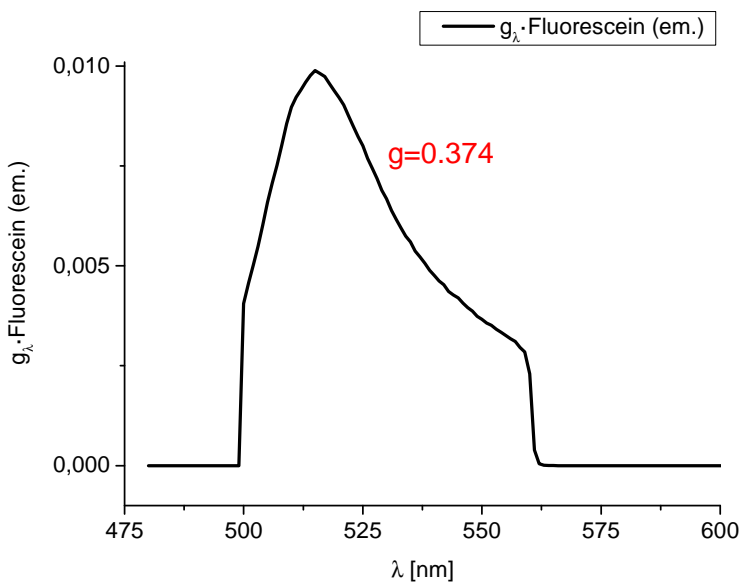


Figure S4: Measured transmission function g_λ multiplied with the fluorescence emission spectrum of Fluorescein in 0.1 M NaOH (black). In red the integrated transmission parameter g is given, stating that a fraction of 37.4% of the fluorescence emission is actually measured (not taking into account the CEF of the objective).

3 Theoretical Foundation of the τ -Method

The τ -method exploits the linear relation between the fluorescence lifetime and the fluorescence QY. This relation is derived from the definition of QY in terms of rate constants:¹⁴

$$QY = \frac{k_f}{k_f + k_{nr}}, \quad (\text{S17})$$

where k_f is the fluorescence emission rate and k_{nr} encloses all the non radiative de-excitation rates. Common non radiative de-excitation pathways are: (i) collisional quenching, (ii) inter-system crossing, and (iii) Förster resonance energy transfer between a donor and an acceptor dye. The respective rate constants are (i) $k_Q \cdot [Q]$, (ii) k_{isc} , and (iii) k_{ET} . By using the definition of lifetimes $\tau = \frac{1}{k_f + k_{nr}}$ and by defining the natural lifetime of the fluorophores as $\tau_n = \frac{1}{k_f}$, a new expression for the QY is obtained from Equation S17

$$QY = \frac{\tau}{\tau_n} \quad (\text{S18})$$

showing that the QY is linearly dependent on the fluorescence lifetime. When the fluorophore is embedded in a complex environment, a discrete distribution of radiative and non-radiative rates is generally observed.² Then, the measured QYs are the sum of the QYs of individual states (QY_i) weighted by their relative populations x_i , i.e. an ensemble average:

$$\langle QY \rangle = \sum_i x_i \cdot QY_i. \quad (\text{S19})$$

By using Equation S18, and the definition of amplitude averaged lifetime $\langle \tau \rangle = \sum_i x_i \cdot \tau_i$, Equation S19 becomes

$$\langle QY \rangle = \sum_i \frac{x_i \cdot \tau_i}{\tau_n} = \frac{\langle \tau \rangle}{\tau_n} \quad (\text{S20})$$

Here, the amplitude and lifetime components (x_i and τ_i) are obtained from fits of multiexponential fluorescence decays. Unfortunately, the absolute estimation of the QY with Equation

S18 or S20 is not feasible in practice. Indeed, the proportionality constant $1/\tau_n$ is not easily determined. The solution is to calculate the ratio of the lifetimes of an "unknown" (S) and a reference (R) sample with almost the same natural lifetimes ($\tau_n^S \simeq \tau_n^R$)

$$\langle QY_S \rangle \simeq \frac{\langle \tau \rangle_S}{\langle \tau \rangle_R} \cdot \langle QY_R \rangle. \quad (\text{S21})$$

This equation is used to estimate the QYs with the τ -method. According to Equation S21, the applicability of the τ -method is limited to the comparison of samples with similar natural lifetimes. Practically, this means that S and R must be the same fluorophore embedded in different environments. The best situation is when a bound fluorophore is compared to the unbound homologue. For simplicity, in the main text the ensemble average notation $\langle \dots \rangle$ is discarded.

4 Experiments and Data analysis

4.1 “Low-excitation” intensity regime

The resulting parameters concerning the setup used in this work are summarized in Table S1. $P_{0,max}$ denotes the laser power corresponding to $2 \frac{kW}{cm^2}$. The results correspond to the case of continuous excitation.

Table S1: Setup parameters needed to predict the upper boundary of the “low-excitation” intensity regime, $P_{0,max}$. λ_{ex} denotes the excitation wavelength of the laser and ω denotes the waist of the unfocused laser beam. ω_0 is the waist of the focused laser beam and f is the focal length of the objective.

λ_{ex} [nm]	ω [mm]	ω_0 [nm]	$P_{0,max}$ [μ W]	f [mm]
487	2.1	222	1.55	3
637	2.1	290	2.64	3

4.2 Results of the MB-method

The measurements were performed as follows. For each sample, the MB were measured at different intensities in the “low-excitation” regime. The MB were plotted as a function of the corresponding intensities. Then, the slope m was determined by linear least-squares fitting, whereas the fitted line was constrained to cross the origin. For the proof-of-principle measurements using free fluorophores, three to five data points were recorded in order to determine the lowest number of data points required to determine accurate QYs. All following measurements were performed applying three different excitation intensities only. All solutions were diluted to have around 3 to 10 fluorescent particles in the illumination volume to keep the signal-to-noise ratio high. In the case of the Tryptophane-quenching measurements the number of fluorescent particles was chosen to be smaller than 0.5 to test the performance of the method at “single-molecule” concentrations. Pure fluorophore samples were measured using continuous excitation. All other measurements were performed using pulsed-excitation with a frequency $f = 20$ MHz. All time traces were recorded for five minutes. The results

of all measurements are summarized in Table S2.

Table S2: Overview of parameters relevant for the MB-method; reference fluorophores given in red

sample	g	$\epsilon_{\lambda_{max}}$ [M ⁻¹ cm ⁻¹]	m [cpm/sI]	QY
Fluorescein in 0.1M NaOH	0.374	73743	3746 ± 86	0.92
Atto488 in water	0.387	55653	2321 ± 70	0.73 ± 0.03
Alexa488 in PBS	0.380	66121	3406 ± 104	0.92 ± 0.04
Alexa488 in PBS	0.387	52414	4794 ± 161	0.92
PGK D256C-Alexa488 in MOPS	0.395	47036	3629 ± 50	0.76 ± 0.03
PGK T202C-Alexa488 in MOPS	0.397	43910	3315 ± 185	0.74 ± 0.05
Alexa647 in PBS	0.429	159208	7601 ± 294	0.33
PGK D256C-Alexa647 in MOPS	0.448	120211	9366 ± 351	0.52 ± 0.03
PGK T202C-Alexa647 in MOPS	0.438	141949	9675 ± 287	0.46 ± 0.02
Alexa488 in PBS	0.380	52414	3254 ± 127	0.92
Alexa488 in 10mM Trp	0.386	52959	2676 ± 86	0.74 ± 0.04
Alexa488 in 20mM Trp	0.386	52959	2093 ± 69	0.58 ± 0.03
Alexa488 in 26mM Trp	0.386	52959	1742 ± 119	0.48 ± 0.04

4.3 Results of the τ -method

To determine the fluorescence lifetime τ of a sample, TCSPC-histograms of the parallelly (I_{\parallel}) and perpendicularly (I_{\perp}) polarized fluorescence emission component with respect to the polarization of the excitation light were recorded. As was shown by Fisz,¹⁵ employing a high-numerical aperture objective the unpolarized fluorescence intensity decay is well-approximated by:

$$I_{unp} = I_{\parallel} + G \cdot I_{\perp} \quad (\text{S22})$$

Here, a polarizing beam-splitter cube was used to be able to measure both polarization components simultaneously. G accounts for differences in the detection efficiency between the two detection channels.² Data-sets were analyzed by fitting mono- or bi-exponential decays to the recorded TCSPC-histograms using the method of non-linear least-squares minimization. The goodness-of-fit was judged on the basis of the reduced χ^2 -value and the course of the residuals. The instrument response function (IRF) of the setup was taken into account via iterative re-convolution. The IRF was measured using Atto655 and Atto488

dissolved in saturated potassium iodide solutions. All TCSPC histograms were recorded until their peak reached a value of at least 30,000 counts.

Table S3: Overview of all outcome parameters concerning the τ -method; reference fluorophores given in red

sample	$\langle\tau\rangle$ [ns]	QY
Alexa488 in PBS	4.11 ± 0.01	0.92
PGK D256C-Alexa488 in MOPS	3.53 ± 0.04	0.78 ± 0.01
PGK T202C-Alexa488 in MOPS	3.49 ± 0.05	0.78 ± 0.01
Alexa647 in PBS	1.01 ± 0.06	0.33
PGK D256C-Alexa647 in MOPS	1.45 ± 0.02	0.47 ± 0.03
PGK T202C-Alexa647 in MOPS	1.36 ± 0.01	0.44 ± 0.03
Alexa488 in PBS	4.08 ± 0.01	0.92
Alexa488 in 10mM Trp	3.48 ± 0.02	0.79 ± 0.01
Alexa488 in 20mM Trp	3.22 ± 0.02	0.73 ± 0.01
Alexa488 in 26mM Trp	3.01 ± 0.02	0.68 ± 0.01

4.4 Derivation of the quenching constants

The collisional (K_c) and static (K_s) quenching constants were obtained by global fitting of the experimentally determined τ_0/τ and MB_0/MB data sets. The following equations were used^{14,16,17}

$$\frac{\tau_0}{\tau} = 1 + K_c [Q] \tag{S23}$$

$$\frac{MB_0}{MB} = (1 + K_c [Q])e^{K_s[Q]}, \tag{S24}$$

respectively. The exponential quenching contribution in Equation S24 can be interpreted with a sphere-of-action model.¹⁶ According to the model, instantaneous quenching takes place when a quencher Q resides within a "sphere of action" of volume $V = \frac{K_s \cdot 1000}{N_A}$ (with the volume in m^3) surrounding the fluorophore at the time of excitation. The radius of the sphere is $r = (3V/4\pi)^{1/3}$.

5 Estimation of the Sample Consumption

One of the advantages of the MB-method with respect to the optical method is the lower sample consumption. To compare the amount of sample consumed by these two methods, the worst case scenario of a fluorophore with low molar absorption coefficient (Alexa 488: $\epsilon = 73,000 \text{ M}^{-1}\text{cm}^{-1}$) is analyzed. First, the concentration regimes accessible by a cuvette-based spectrophotometer and a micro-volume spectrophotometer are calculated. The Beer-Lambert law is used for the purpose

$$c = \frac{OD}{\epsilon \ell}. \quad (\text{S25})$$

Here, ℓ is the path length. Second, the amount of consumed moles n of samples is calculated by multiplying the concentration c by the used sample-solution volume V

$$n = cV. \quad (\text{S26})$$

The results are displayed in Figure S5. Overall, the lowest sample consumption is obtained with a micro-volume spectrophotometer (i.e. $\ell = 0.1 \text{ cm}$ and $V = 2 \mu\text{l}$). If a cuvette-based spectrophotometer is used, the 5 cm cuvette ($V = 3 \text{ ml}$) gives the best results. Therefore, these two options are considered in the following.

To understand the difference between the optical and the MB method, the experimental conditions to be fulfilled to get reliable results must be considered. On the one hand, the accuracy of the optical method relies on the accuracy of the measured ODs. Therefore, low-noise absorption spectra must be measured ($OD_{max} \geq 0.05$). Additionally, the linear dependency of the fluorescence emission on the excitation intensity is only given when $OD_{max} \leq 0.01$. Since the absorption and the fluorescence spectra must be determined at the same concentration, an absorption path length (ℓ_{abs}) greater than the fluorescence path length (ℓ_{fl}) by a factor of $\frac{0.05}{0.01} = 5$ must be used ($\ell_{abs} \geq 5\ell_{fl}$) to overcome this problem. Obviously, this condition precludes the possibility to implement the optical method with a microvolume spectrophotometer because $\ell_{abs} = 0.1 \text{ cm}$ is always lower than $\ell_{flu} = 5 \cdot 0.3 \text{ cm}$

= 1.5 cm. On the other hand, if the MB-method is used, both conditions are easily satisfied by changing the concentration of the sample according to the cuvette path length ($\ell_{fl} = 0.3$ cm and $\ell_{abs} = 0.1/5$ cm).

In this respect, the lowest amount of sample required by the MB-method is given by the values of the blue and black curves at $OD_{max} = 0.05$ (see Figure S5), i.e. 400 pmol and 14 pmol, respectively. Alternatively, the lowest sample amount consumed by the optical method is given by the blue curve value at $OD_{max} = \frac{5.0 \text{ cm}}{0.3 \text{ cm}} \cdot 0.01 \simeq 0.17$, i.e. 1.4 nmol. Therefore, the MB-method reduces the sample consumption by a factor of ~ 3.5 with respect to the optical method. Importantly, this value increases to ~ 100 if a microvolume spectrophotometer is available.

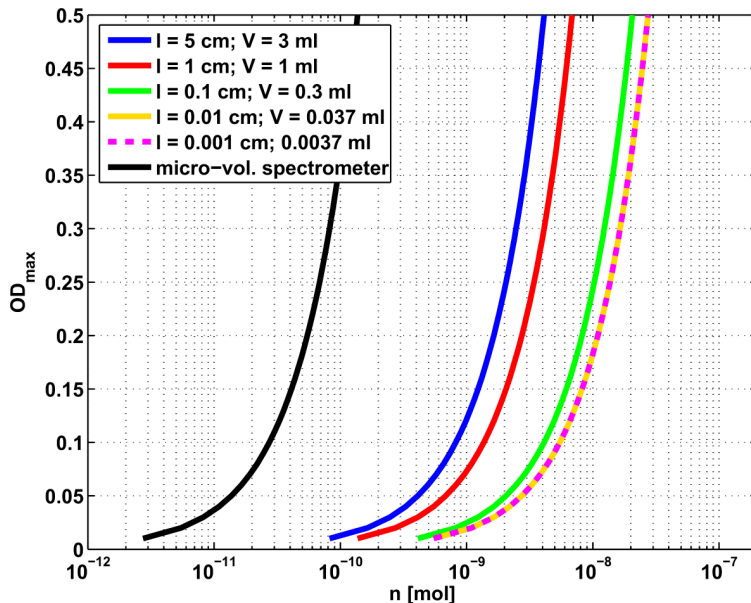


Figure S5: Dependence of the measured OD_{max} from the moles of Alexa 488 as a function of the cuvette path length ℓ_{abs} and volume V (colored lines). The black line was calculated for a microvolume spectrophotometer, i.e. $\ell_{abs} = 0.1$ cm and $V = 2 \mu\text{l}$.

References

- (1) Gregor, I.; Patra, D.; Enderlein, J. Optical Saturation in Fluorescence Correlation Spectroscopy under Continuous-Wave and Pulsed Excitation. *ChemPhysChem* **2005**, *6*.
- (2) Lakowicz, J. *Principles of Fluorescence Spectroscopy*; Springer, 2004.
- (3) Phillips, D.; Drake, R.; O'Connor, D.; Christensen, R. Time Correlated Single-Photon Counting (Tcspc) Using Laser Excitation. *Instrumentat.. Sci. & Tech.* **1985**, *14*, 267–292.
- (4) Schönle, A.; Von Middendorff, C.; Ringemann, C.; Hell, S. W.; Eggeling, C. Monitoring triplet state dynamics with fluorescence correlation spectroscopy: Bias and correction. *Microscopy Research and Technique* **2014**, *77*, 528–536.
- (5) Eggeling, C.; Widengren, J.; Brand, L.; Schaffer, J.; Felekyan, S.; Seidel, C. A. M. Analysis of Photobleaching in Single-Molecule Multicolor Excitation and Frster Resonance Energy Transfer Measurements. *J. Phys. Chem. A* **2006**, *110*, 2979–2995.
- (6) Widengren, J.; Mets, U.; Rigler, R. Fluorescence correlation spectroscopy of triplet states in solution: a theoretical and experimental study. *J. Phys. Chem.* **1995**, *99*, 13368–13379.
- (7) Blom, H.; Chmyrov, A.; Hassler, K.; Davis, L. M.; , J. Triplet-State Investigations of Fluorescent Dyes at Dielectric Interfaces Using Total Internal Reflection Fluorescence Correlation Spectroscopy. *J. Phys. Chem. A* **2009**, *113*, 5554–5566.
- (8) Saleh, B.; Teich, M. *Fundamentals of photonics*; Wiley series in pure and applied optics; Wiley, 1991.
- (9) Koppel, D. E. Statistical accuracy in fluorescence correlation spectroscopy. *Phys. Rev. A* **1974**, *10*, 1938–1945.

- (10) Hess, S. T.; Webb, W. W. Focal Volume Optics and Experimental Artifacts in Confocal Fluorescence Correlation Spectroscopy. *Biophys. J.* **2002**, *83*, 2300 – 2317.
- (11) Elson, E. L.; Magde, D. Fluorescence correlation spectroscopy. I. Conceptual basis and theory. *Biopolymers* **1974**, *13*, 1–27.
- (12) Buschmann, V.; Weston, K. D.; Sauer, M. Spectroscopic Study and Evaluation of Red-Absorbing Fluorescent Dyes. *Bioconj. Chem.* **2003**, *14*, 195–204.
- (13) Widengren, J.; Schwille, P. Characterization of Photoinduced Isomerization and Back-Isomerization of the Cyanine Dye Cy5 by Fluorescence Correlation Spectroscopy. *J. Phys. Chem. A* **2000**, *104*, 6416–6428.
- (14) Lakowicz, J. R. *Principles of Fluorescence Spectroscopy - Second Edition*; Kluwert Academic/Plenum Publ.: New York, USA, 1999.
- (15) Fisz, J. J. Fluorescence Polarization Spectroscopy at Combined High-Aperture Excitation and Detection: Application to One-Photon-Excitation Fluorescence Microscopy. *J. Phys. Chem. A* **2007**, *111*, 8606–8621.
- (16) Eftnik, M.; Ghiron, C. Fluorescence quenching of indole and model micelle systems. *J. Phys. Chem.* **1976**, *80*, 486–493.
- (17) Doose, S.; Neuweiler, H.; Sauer, M. A close look at fluorescence quenching of organic dyes by tryptophan. *ChemPhysChem* **2005**, *6*, 2277–2285.